International Journal of Aeronautical and Space Sciences (2021) 22:1154–1169
https://doi.org/10.1007/s42405-021-00394-8

ORIGINAL PAPER

Stability Margin and Structural Coupling Analysis of a Hybrid INDI Control for the Fighter Aircraft

Chong-Sup Kim[1] · Chang-Ho Ji[2] · Gi-Oak Koh[1] · Byoung Soo Kim[3]

Received: 18 December 2020 / Revised: 6 May 2021 / Accepted: 3 June 2021 / Published online: 21 July 2021

Abstract
The sensor-based incremental nonlinear dynamic inversion (INDI) using angular acceleration measured by inertial measurement unit (IMU) sensor is a very robust control method on various model uncertainties when the aircraft maneuvers with moderate angle-of-attack (AoA) and high gravity in transonic speed flight conditions. However, the measured angular acceleration has time delay characteristics due to actuator and aircraft dynamics, IMU sensor dynamics, differential angular rate and structural coupling filter (SCF) and so on. These characteristics of angular acceleration feedback reduce dramatically the stability margin of the control system. In this paper, we propose the synchronization filter design method of the control surface feedback path for improving stability margin, based on the proposed hybrid INDI control method using error between the angular acceleration measured from IMU sensor and the angular acceleration calculated from on-board model (OBM) and control surface feedback. To evaluate the proposed control method, we perform the frequency-domain linear analysis and the time-domain simulation. As a result of the evaluation, synchronization method of control surface feedback not only improves the stability margin characteristics of the control system but also eliminates the structural coupling in low frequency range by designing the control surface command feedback using actuator command which is the output of flight control computer (FLCC).

Keywords Stability margin · Hybrid incremental nonlinear dynamic inversion (INDI) · Fighter aircraft

List of Symbols

$\mathbf{x}$	State vector
$\mathbf{u}$	Control input vector
f	Nonlinear state dynamic function
g	Nonlinear control distribution function
$\Delta\mathbf{u}$	Incremental control command (°)
$\Delta\mathbf{d}$	Virtual control command (°)
$\mathbf{u}_0$	Previous control command (°)
K_{aug}	Additional augmentation control gain
f_{obm}	Nonlinear state dynamic function of OBM
g_{obm}	Nonlinear control distribution function of OBM
$\dot{\mathbf{x}}_{\mathrm{des}}$	Rate of desired state vector (°/s^2)
$\dot{\mathbf{x}}_{\mathrm{obm}}$	Rate of state vector calculated from OBM (°/s^2)
$\dot{\mathbf{x}}_{\mathrm{add}}$	Rate of state vector of additional augmentation control sensor (°/s^2)
K_{ni}	Integral gain to normal acceleration
K_{np}	Proportional gain to normal acceleration feedback
K_f	Feed-forward gain
K_q	Proportional gain to pitch rate feedback
$T_{\theta 2}^{\mathrm{des}}$	Desired pitch attitude time constant
$T_{\theta 2}$	Pitch attitude time constant
K_{pfn}	Pilot prefilter numerator gain
K_{pfd}	Pilot prefilter denominator gain
ζ	Short-period damping ratio
ω	Short-period frequency (rad)
V_T	True speed (ft/s)
M_k	Pitching moment of k
δ_{es}	Elevator deflection (°)
α_m	Measured angle-of-attack (°)
q_m	Measured pitch rate (°/s)
I_{ii}	Principal moment of inertia (slug-ft^2) ($i = x, y, z$)

✉ Chong-Sup Kim
robocskim@koreaaero.com

[1] Flight Control Law Team, Korea Aerospace Industries, Ltd., Gyeongsangnamdo, Sacheon 52529, Korea

[2] Flight Control Test Team, Korea Aerospace Industries, Ltd., Gyeongsangnamdo, Sacheon 52529, Korea

[3] School of Aerospace and Software Engineering, Gyeongsang National University, Gyeongsangnamdo, Jinju 52725, Korea

I_{ij}	Production moment of inertia (slug-ft^2) ($i=x, y, z, j=x, y, z$)
M_k^z	Pitching moment for k of z ($k=\alpha, q, \delta_{es}$, $z=$obm, ac)
$\dot{q}_m$	Pitch angular acceleration from sensor (°/s^2)
$\dot{q}_{obm}$	Pitch angular acceleration from OBM (°/s^2)
$\dot{q}_{add}$	Pitch angular acceleration from additional augmentation control (°/s^2)
H_{syn}	Synchronization filter
H_1^{total}	AoA and IMU sensor models with aircraft dynamics
H_2^{total}	Angular acceleration sensor model with aircraft dynamics
ω_{syn}	Natural frequency of synchronization filter (rad)
ζ_{syn}	Damping ratio of synchronization filter

Abbreviations

IMU	Inertial measurement unit
SCF	Structural coupling filter
SCT	Structural coupling test
INDI	Incremental nonlinear dynamic inversion
CONDUIT	Control designer's unified interface
OBM	On-board model
PID	Proportional-integral-derivatives
NASA	National aeronautics and space administration
HARV	High angle-of-attack research vehicle
RESTORE	Reconfigurable control for tailless aircraft
STOVL	Short take-off/vertical landing
VAAC	Vectored thrust aircraft advanced control
NLR	Netherlands aerospace centre
DLR	German aerospace center
LE	Leading edge
LOES	Low-order equivalent system
CA	Control allocation
FLCS	Flight control system
DFBW	Digital fly-by-wire
FLCC	Flight control computer
RSS	Relaxed static stability

1 Introduction

Prior to the 1990s, the design method of flight control law for production fighter aircraft adopted the classical control theories such as proportional-integral-derivatives (PID) [1, 2]. In recent years, modern highly maneuverable fighter aircraft have applied more advanced multivariable control techniques to flight control law design to improve flying and handling qualities. The model or sensor-based incremental nonlinear dynamic inversion (INDI) [3] which is based on calculated or measured angular acceleration has been the most popular multivariable control technique. The advantage of the model-based INDI with classical control techniques is that nonlinearities of aerodynamics directly are incorporated into the control laws without gain scheduling, and separates the flying qualities dependent part and the airframe-dependent part in the control laws [4]. This control method permits traditional specification such as MIL-STD-1797A [5] to be directly applied as a design approach for airworthiness certification that is required in the development of the aircraft aimed to production. And, it ultimately improves aerodynamic performance and handling qualities of the aircraft, and reduces development cost and period as long as it is possible to secure accurate aerodynamic data. Whereas, drawback of the model-based INDI which is based on the predicted angular acceleration from on-board model (OBM) and control surface command feedback is that model and airdata uncertainties can degrade handling qualities and even destroy the flight safety of the aircraft under unstable situations [6].

As an attractive to solving these issues, the application of the sensor-based INDI which is based on the measured angular acceleration from IMU sensor became visible. The sensor-based INDI has the advantage of robustness characteristics on various model uncertainties but it has drawback of reducing the stability margin of control system on time delay of the measured angular acceleration due to measurement systems such as differentiator, actuator and sensor dynamics, and a lower control system sampling time [6–8]. In addition, structural noise of control surfaces command feedback has the characteristics of reducing the gain margin in low and medium frequency range during structural coupling test (SCT).

Recently, the INDI has been extensively studied and applied to demonstration and production aircraft. The development of the model-based NDI control in aerospace industry started in national aeronautics and space administration (NASA) with the participation of Honeywell, Boeing, and Lockheed Martin in early 1990s. The use of the model-based NDI as a viable control law methodology has been demonstrated in the restricted flight envelope on various flight control research aircrafts such as F-18 high angle-of-attack research vehicle (HARV) [9], X-38 [10, 11], X-36 reconfigurable control for tailless aircraft (RESTORE) [12], and X-35B short take-off/vertical landing (STOVL) [13]. In addition, F-35 joint strike fighter (JSF) [14] was the first production fighter incorporating the model-based INDI in the entire flight envelopes. Moreover, the sensor-based INDI which uses the measured angular acceleration and control surface positions as feedback parameters was evaluated on vectored thrust aircraft advanced control (VAAC) Harrier [15, 16] in 1999. In 2000, NASA applied this control method to innovative control effector tailless aircraft [17]. Recently, The Netherlands Aerospace Centre (NLR) and german aerospace center (DLR) with the Technical University of Delft have applied it to Cessna 550 demonstrator [18] and have proved the performance of the developed control law. The stability and robustness of the sensor-based INDI control has already been proven [19, 20].

Recently, Kim et al. [21–25] has the proposed hybrid INDI control method which feedbacks the measured and calculated angular accelerations in highly unstable flight and transonic flight regime. In the flight conditions where wing flow separation occurs due to the unstable flow field, the symmetrical or asymmetrical flow separation may generate a sudden large imbalance in lift between wing panels [26, 27]. These effects generate unexpected aircraft motions that degrade flying qualities and performance of the aircraft, threaten the pilot's health, overstress the aircraft structure and lead to instability of the structural load for a turning flight with high gravity. Above all, modeling these effects mathematically on basis of aerodynamic data is very difficult in these flight characteristics because the dynamic behavior is unpredictable and irregular. These characteristics are caused by highly nonlinear aerodynamic behavior in which flow separation occurs on the leading edge (LE) of the wing and destroys lift behind the center-of-gravity position in high speed and moderate AoA [28]. Due to general nonlinear aerodynamic behavior in these flight conditions, unexpected motions occur rapidly and heavily in attitude and normal acceleration while reducing flying qualities of the aircraft considerably. To solve this problem, various configuration design methods such as vertex generator, wing fence, LE slat, LE airfoil modification and wing-body strakes have been proposed which can be adopted the aircraft in the early development stage. These configuration design methods have been used in the aircraft such as F-84, F-86, G-91, A-4, T-45, and F-111 development program [26, 29–36]. And, there are the feed-forward control methods such as leading- and trailing-edge flap scheduling as ways of minimizing flow separation by optimizing the wing airfoil. These feed-forward control methods [37–54] have been applied to the aircraft such as F-8, F-4, Harrier and F-18. The modern fighter aircrafts have adopted these feed-forward control methods as the basis. As already known, unexpected motion can be solved up to 80% with applying only both the configuration design and the feed-forward control methods. Additionally, there are the feedback control methods to minimize unexpected motion by augmenting the damping characteristics of the aircraft by feeding back the various state variables of the aircraft in the closed loop control. Recently, some effort has been made to these feedback control methods using optimal control [55, 56], adaptive and neural network control [55, 56] theories to improve the unexpected motions. However, it is difficult to obtain airworthiness certification since this control method does not provide a deterministic solution. That is, it is limited method to apply these control methods to the aircrafts aiming to production which necessarily requires airworthiness certification. The proposed hybrid INDI control method is known to improve the handling qualities and instantaneous turn rate performance by reducing the unexpected motions on sudden large imbalance in lift of the aircraft. However, time delay of measured angular acceleration reduces the stability margin of the control system. To improve the stability margin of control system, we propose the synchronization filter design method minimizing structural noise of control surfaces and time delay of measured angular acceleration.

The main contribution of this paper can be summarized as follows. Firstly, the hybrid INDI control method which can be implemented by adding to the existing configuration design methods can more effectively reduce the unexpected motions of the aircraft on model uncertainties and nonlinearities at transonic flight regime. Secondly, this control method provides a deterministic solution to obtain the airworthiness certification, based on the proven the model-based INDI control. Thirdly, the proposed synchronization filter of control surface feedbacks effectively improves the stability margin of control system as a simple design method which minimizes flight control computer (FLCC) throughput. Lastly, the proposed control surface incremental method effectively increases the gain margin of control system by reducing the structural vibration control surfaces of the aircraft in the low and medium frequency range.

The rest of this paper is organized as follows. Section 2 describes the hybrid INDI control theory including synchronization filter design based on this additional augmentation control. Section 3 describes the evaluation flight conditions and methods and shows the evaluation results for the proposed control methods with frequency-domain stability evaluation to verify structural coupling effect on control surface feedback position and synchronization filter, and time-domain nonlinear simulation based on the mathematical model of the advanced trainer. And, Sect. 4 presents conclusions and future plans.

2 Control Law Design

Figure 1 shows the control structure of the hybrid INDI control law with additional augmentation control feeding back error between the angular acceleration measured from IMU sensor and the angular acceleration calculated form OBM and represents decoupling between flying quality-dependent portions and airframe-dependent portion. The desired angular acceleration ($\dot{\mathbf{x}}_{des}$) is calculated from desired dynamics which reflects how the aircraft should fly in response to the pilot input. The desired dynamics consists of command shaping and regulator. The command shaping aims to translate the pilot's control stick input to the desired aircraft movement, while the regulator aims to directly set the low-order equivalent system (LOES) parameter values such as short-period mode damping

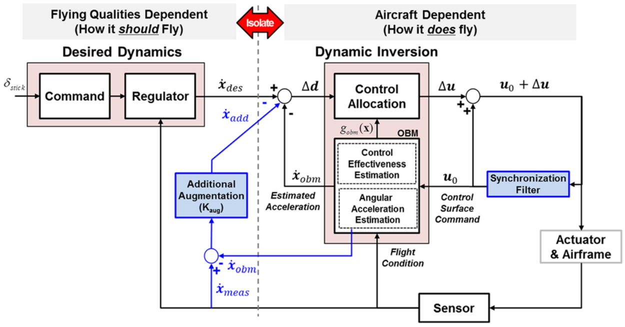

Fig. 1 Control structure of the hybrid INDI control law with additional augmentation control

and frequency to comply with the classical flying qualities criteria when the aircraft is achieving this motion. The airframe-dependent portion comprises OBM and control allocation (CA). The OBM provides the estimated angular acceleration to calculate the dynamic inversion and control effectiveness matrix to compute CA.

The nonlinear dynamic equation of motion can be expressed as

$$\dot{\mathbf{x}} = F(\mathbf{x}, \mathbf{u}), \tag{1}$$

where $\mathbf{x} \in R^n$, is the state vector and $\mathbf{u} \in R^m$ is the control input vector. In general, the state vector includes the angular velocity of the aircraft. For conventional uses where small perturbations form trim conditions, the function F is linear in $\mathbf{u}$. Equation (1) can be rewritten as

$$\dot{\mathbf{x}} = f(\mathbf{x}) + g(\mathbf{x})\mathbf{u}, \tag{2}$$

where, f is a nonlinear state dynamic function and g is a nonlinear control distribution function. Considering the model-based INDI control, if actual control command $\mathbf{u}$ is defined as the sum of previous control command $\mathbf{u}_0$ and incremental control command $\Delta\mathbf{u}$, Eq. (2) can be shown as Eq. (3).

$$\dot{\mathbf{x}} = f(\mathbf{x}) + g(\mathbf{x})\left(\mathbf{u}_0 + \Delta\mathbf{u}\right). \tag{3}$$

If we assume $g(\mathbf{x})$ is invertible for all values of $\mathbf{x}$, Eq. (3) can be summarized as Eq. (4)

$$\Delta\mathbf{u} = g_{\mathrm{obm}}^{-1}(\mathbf{x})\left\{\dot{\mathbf{x}} - \left(f_{\mathrm{obm}}(\mathbf{x}) + g_{\mathrm{obm}}(\mathbf{x})\mathbf{u}_0\right)\right\}, \tag{4}$$

where $f_{\mathrm{obm}}(\mathbf{x}) + g_{\mathrm{obm}}(\mathbf{x})\mathbf{u}_0$ is angular acceleration, $\dot{\mathbf{x}}_{\mathrm{obm}}$ calculated from OBM. We will specify $\dot{\mathbf{x}}$ as the rate of the desired states $\dot{\mathbf{x}}_{\mathrm{des}}$ to achieve the flying qualities design goals defined by the designer. By swapping $\dot{\mathbf{x}}$ in the previous equation to $\dot{\mathbf{x}}_{\mathrm{des}}$, Eq. (4) can be arranged Eq. (5).

$$\Delta\mathbf{u} = g_{\mathrm{obm}}^{-1}(\mathbf{x})\left\{\dot{\mathbf{x}}_{\mathrm{des}} - \dot{\mathbf{x}}_{\mathrm{obm}}\right\}. \tag{5}$$

Consequently, current control command $\mathbf{u}_{\mathrm{cmd}}$ can be designed by combining the previous control command and the increment control command, as shown in Eq. (6)

$$\mathbf{u}_{\mathrm{cmd}} = \mathbf{u}_0 + \Delta\mathbf{u}. \tag{6}$$

By substituting Eq. (5) into Eq. (3), the dynamic characteristics of the aircraft can be completely canceled in case of $g_{\mathrm{obm}}(\mathbf{x}) \approx g(\mathbf{x})$ and $f_{\mathrm{obm}}(\mathbf{x}) \approx f(\mathbf{x})$ and the desired angular acceleration of the aircraft can be obtained as

$$\dot{\mathbf{x}} = f(\mathbf{x}) + g(\mathbf{x})\left\{\mathbf{u}_0 + g_{\mathrm{obm}}^{-1}(\mathbf{x})\left(\dot{\mathbf{x}}_{\mathrm{des}} - \dot{\mathbf{x}}_{\mathrm{obm}}\right)\right\} = \dot{\mathbf{x}}_{\mathrm{des}}. \tag{7}$$

Note also that if the exact aircraft model can be obtained, the desired dynamics that depends on the flying qualities requirements can also be designed without considering the aircraft dynamics. However, it is impossible to obtain the exact aircraft model due to several models such as computational time delay and actuator and sensor dynamics in control system. As these factors increase order of control system due to the complex models, they also increase the errors between the aircraft model and the flying qualities requirements represented in first- or second-order models. This means that the control gains in desired dynamics must be adjusted according to the off-line optimization procedure to compensate for the uncertainties of aircraft dynamics.

2.1 Desired Dynamics

Figure 2 shows the detailed structure of the hybrid INDI control in longitudinal axis. The architecture of the desired dynamics is shown in Fig. 2b, where response type is selected as normal acceleration command ($n_{z,\mathrm{cmd}}$) in focus of gross acquisition. In addition, desired dynamics is designed based on a proportional-plus-integral (PI) type with normal acceleration ($n_{z,m}$) and pitch rate (q_m) as feedback variables. Moreover, the feed-forward control loop and command shaping prefilter are designed to enhance the initial pitch angular acceleration response and handling qualities while maneuvering aggressively. The control gains in desired dynamics are scheduled with Mach number and altitude to ensure a satisfactory level of flying qualities within all flight envelopes [57].

The initial value of the flying quality parameters (K_{ni}, K_q, K_{np} and K_f) can be obtained as

$$K_{\mathrm{ni}} = \frac{g_0}{V_T}\omega^2, K_q = 2\zeta\omega, K_{\mathrm{np}} = \frac{g_0}{V_T}T_{\theta 2}\omega^2, K_f = \frac{g_0}{V_T}T_{\theta 2}\omega^2, \tag{8}$$

where ζ and ω represent the damping ratio and natural frequency of the short-period mode and V_T is the aircraft true speed (ft/s), g_0 is the gravitational acceleration (g), and $T_{\theta 2}$ is the pitch attitude time constant, which can be obtained from the aircraft dynamics.

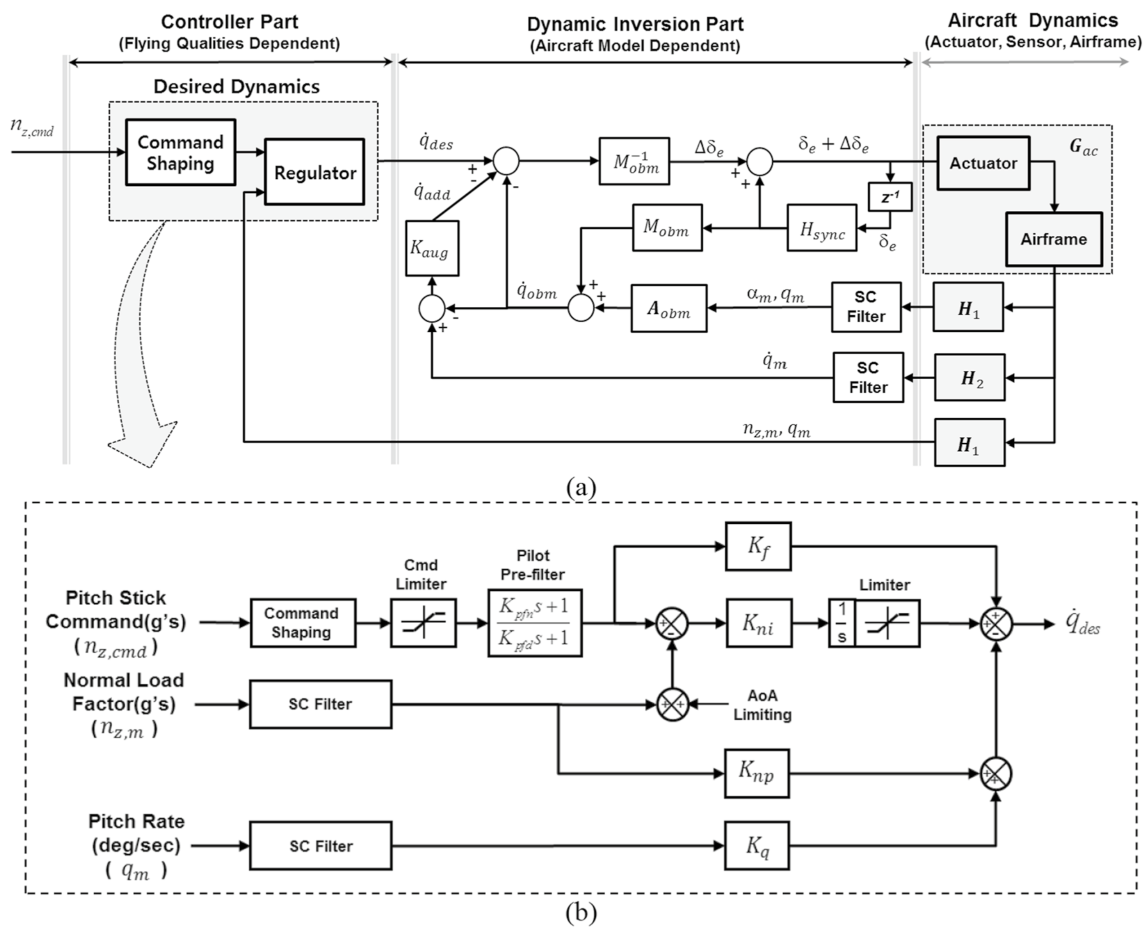

Fig. 2 Structure of the hybrid INDI control in longitudinal axis. **a** Overall the hybrid INDI control law architecture. **b** Detailed architecture of desired dynamics [57]

This lead filter is designed in the pilot command loop to improve the handling qualities. Thus, Eq. (9) represents the pilot prefilter.

$$\frac{T_{\theta 2}^{\mathrm{des}} s + 1}{T_{\theta 2} s + 1} = \frac{K_{\mathrm{pfn}} s + 1}{K_{\mathrm{pfd}} s + 1}. \tag{9}$$

2.2 Dynamic Inversion

In general, the longitudinal equations of motion can be expressed as Eq. (10).

$$\dot{q} = \frac{1}{I_{yy}}\left[M + \left(I_{zz} - I_{xx}\right)pr + I_{xz}\left(r^2 - p^2\right)\right], \tag{10}$$

where p and r (°/s^2) are the angular velocities of the aircraft, I_{xx}, I_{yy} and I_{zz} are the principal moments of inertia and I_{xz} is the product of inertia. Now, we will assume the longitudinal moment M is linear with respect to aerodynamic derivatives, i.e.,

$$M = M_{\alpha}\alpha + M_q q + M_{\delta_{\mathrm{es}}}\delta_{\mathrm{es}}, \tag{11}$$

where M_{α}, M_q and $M_{\delta_{\mathrm{es}}}$ are linearized moments due to aerodynamic forces and δ_{es} is the symmetric deflection of the horizontal tails. By substituting the above linear moment equation Eq. (11) into Eq. (10), we can obtain the relation in Eq. (12) that combines linear and nonlinear terms.

$$\dot{q} = M'_{\alpha}\alpha + M'_q q + M'_{\delta_{\mathrm{es}}}\delta_{\mathrm{es}} + \frac{1}{I_{yy}}\left[\left(I_{zz} - I_{xx}\right)pr + I_{xz}\left(r^2 - p^2\right)\right], \tag{12}$$

where M_k' is a linearized moment due to aerodynamic forces and can be defined as

$$M_k' = \frac{1}{I_{yy}} M_k, k = \alpha, q, \delta_{\mathrm{es}}. \tag{13}$$

If the last term is ignorable in Eq. (12), the result is identical to the linear set of DI equations.

Finally, inverting the above equation as well as applying the commanded, desired, and measured values gives the resulting NDI control.

$$\delta_{es}^{cmd} = \frac{1}{M_{\delta_{es}}^{obm}} \left\{ \dot{q}_{des} - \left(M_{\alpha}^{obm} \alpha_m + M_q^{obm} q_m \right) - \frac{1}{I_{yy}} \left[\left(I_{zz} - I_{xx} \right) p_m r_m + I_{xz} \left(r_m^2 - p_m^2 \right) \right] \right\}. \tag{14}$$

2.3 Additional Augmentation

In the control structure of Fig. 2a, the pitch angular acceleration calculated from OBM ($\dot{q}_{obm}$), the pitch angular acceleration obtained from additional augmentation control ($\dot{q}_{add}$) and the virtual pitch control command (Δd) are given as

$$\dot{q}_{obm} = M_{\alpha}^{obm} \alpha_m + M_q^{obm} q_m + M_{\delta_{es}}^{obm} \delta_{es}, \tag{15}$$

$$\dot{q}_{add} = K_{aug} \left(\dot{q}_m - \dot{q}_{obm} \right), \tag{16}$$

$$\Delta d = \dot{q}_{des} - \dot{q}_{obm} - \dot{q}_{add}, \tag{17}$$

where K_{aug} is the control gain of additional augmentation control and has an arbitrary value between 0.0 and 1.0. By substituting from Eqs. (15–17) into Eq. (6), the current pitch control command can be obtained as

$$\delta_{es} = \delta_{es,0} + \frac{1}{M_{\delta_{es}}^{obm}} \left[\dot{q}_{des} - \left\{ K_{aug} \dot{q}_m + \left(I - K_{aug} \right) \dot{q}_{obm} \right\} \right], \tag{18}$$

where the term of $K_{aug} \dot{q}_m + \left(I - K_{aug} \right) \dot{q}_{obm}$ means to proportionally use $\dot{q}_m$ and $\dot{q}_{obm}$ according to the value of K_{aug}. By substituting from Eq. (18) into Eq. (2), the dynamic equation of motion including control law can be expressed as

$$\dot{q} = M_{\alpha}^{ac} \alpha_m + M_q^{ac} q_m + M_{\delta_{es}}^{ac} \delta_{es} + \left[\dot{q}_{des} - \left\{ K_{aug} \dot{q}_m + \left(I - K_{aug} \right) \dot{q}_{obm} \right\} \right]. \tag{19}$$

Generally, the model-based INDI control is a control synthesis technique in which the inherent dynamics of a dynamical system is canceled out and is replaced with the desired dynamic selected by control law designer. However, the plant dynamics cannot be modeled exactly in real world, thereby preventing an exact replacement of the inherent plant dynamics with the desired dynamics.

$$\begin{aligned} \min\left\{ e_m, e_{obm} \right\} &\le M_{\alpha}^{ac} \alpha_m + M_q^{ac} q_m + M_{\delta_{es}}^{ac} \delta_{es} \\ &- \left[\left\{ K_{aug} \dot{q}_m + \left(I - K_{aug} \right) \dot{q}_{obm} \right\} \right] \le \max\left\{ e_m, e_{obm} \right\}. \end{aligned} \tag{20}$$

The error of the aircraft model is given by

$$e_m = \left(M_{\alpha}^{ac} \alpha_m + M_q^{ac} q_m + M_{\delta_{es}}^{ac} \delta_{es} \right) - \dot{q}_m, \tag{21}$$

$$e_{obm} = \left(M_{\alpha}^{ac} \alpha_m + M_q^{ac} q_m + M_{\delta_{es}}^{ac} \delta_{es} \right) - \dot{q}_{obm}. \tag{22}$$

2.4 Control Surface Synchronization

The IMU sensor is never infinitely fast, which degrade performance, and necessitates the use of synchronization filter. This section describes the synchronization filter design method. In the hybrid INDI control approach, the feedback for angular acceleration is assumed to be a linear combination of the measured angular acceleration from IMU sensor measurements and the estimated angular acceleration from OBM. The complete transfer function from the desired control input to the elevator control command is given by:

$$\frac{\delta_{es}}{q_{des}} = \frac{G_{ac}^{\delta_{es}}}{\left\{ \dot{q}_{fb} - M_{\delta_{es}}^{obm} H_{syn} \delta_{es} \right\} e^{-\delta T} + M_{\delta_{es}}^{obm}}, \tag{23}$$

where H_{syn} is synchronization filters and order of elements are 2nd or 4th. And total pitch angular acceleration feedback $\dot{q}_{fb}$ can be expressed as

$$\begin{aligned} \dot{q}_{fb} &= K_{aug} \dot{q}_m + \left(I - K_{aug} \right) \dot{q}_{obm} \\ &= K_{aug} \left\{ \left(M_{\alpha}^{ac} \alpha_m + M_q^{ac} q_m \right) H_2^{total} + M_{\delta_{es}}^{ac} H_2^{total} \right\} \\ &+ \left(I - K_{aug} \right) \left\{ \left(M_{\alpha}^{obm} \alpha_m + M_q^{obm} q_m \right) H_1^{total} + M_{\delta_{es}}^{obm} H_{syn} \delta_{es} \right\}, \end{aligned} \tag{24}$$

where H_1^{total} is AoA and IMU sensor models, and H_2^{total} is angular acceleration sensor model including aircraft and actuator dynamics where the control surface command is fed back from control law in FLCC. If the control surface command is fed back from actuator dynamics, H_2^{total} does not include actuator dynamics. Considering the denominator of Eq. (23) by substituting from Eq. (24) into Eq. (16).

$$\begin{aligned} D_u = &\left\{ K_{aug} \left(M_{\alpha}^{ac} \alpha_m + M_q^{ac} q_m \right) H_2^{total} + \left(I - K_{aug} \right) \left(M_{\alpha}^{obm} \alpha_m + M_q^{obm} q_m \right) H_1^{total} \right\} e^{-\delta T} \\ &+ \left\{ K_{aug} M_{\delta_{es}}^{ac} H_2^{total} + \left(I - K_{aug} \right) M_{\delta_{es}}^{obm} H_{syn} - M_{\delta_{es}}^{obm} H_{sync} \right\} \delta_{es} e^{-\delta T} + M'_{\delta_{es}}. \end{aligned} \tag{25}$$

In particular, the following terms require special attention.

$$\Gamma = K_{aug} M_{\delta_{es}}^{ac} H_2^{total} + \left(I - K_{aug} \right) M_{\delta_{es}}^{obm} H_{syn} - M_{\delta_{es}}^{obm} H_{syn}. \tag{26}$$

These additional dynamics, which arise uniquely for the sensor-based INDI, have a direct impact on the broken-loop inversion response and can play an important role in the distortion of the stability margins of the complete control law.

$$H_{\mathrm{syn}} = \frac{K_{\mathrm{aug}} M^{\mathrm{ac}}_{\delta_{\mathrm{es}}}}{M^{\mathrm{obm}}_{\delta_{\mathrm{es}}} - \left(I - K_{\mathrm{aug}}\right) M^{\mathrm{obm}}_{\delta_{\mathrm{es}}}} H_2^{\mathrm{total}}(\Gamma = 0;). \tag{27}$$

Assuming an ideal on-board representation of the control effectiveness ($M^{\mathrm{obm}}_{\delta_{\mathrm{es}}} \approx M^{\mathrm{ac}}_{\delta_{\mathrm{es}}}$), these effects can be eliminated by carefully matching, i.e. synchronizing, the relative phase lag and time delay between the angular acceleration and actuator feedback signals.

Note that if $M^{\mathrm{obm}}_{\delta_{\mathrm{es}}} \neq M^{\mathrm{ac}}_{\delta_{\mathrm{es}}}$, Γ will be nonzero even in case of perfect synchronization. This equation implies that inversion loop distortion effects can only be prevented in case all high-order dynamics represented by actuator model, sensor model, differentiation filter and SCF are taken into account. However, this matching requirement comes at the cost of additional computational complexity. In case computational complexity forms a significant limitation of the control system, alternative, low-order synchronization filter designs can be adopted. However, the fact that $\Gamma \neq 0$ implies that stability margin distortions is inherent to this kind of solutions. The configuration selects a second- and fourth-order low-pass filter with $\zeta_{\mathrm{syn}} = 0.707$ for synchronization purposes. The second-order synchronization filter is applied when the control surface command is fed back at the position after the actuator dynamics, and the fourth-order synchronization filter is applied when the control surface command is fed back before the actuator dynamics.

$$H_{\mathrm{syn}} = \frac{\omega^2_{\mathrm{syn}}}{s^2 + 2\zeta_{\mathrm{syn}}\omega_{\mathrm{syn}}s + \omega^2_{\mathrm{syn}}} \text{ or } \left(\frac{\omega^2_{\mathrm{syn}}}{s^2 + 2\zeta_{\mathrm{syn}}\omega_{\mathrm{syn}}s + \omega^2_{\mathrm{syn}}}\right)^2. \tag{28}$$

This shows that it is possible to develop a full synchronization scheme when combining pure model estimates and angular acceleration sensor values. These synchronization filters improve the stability margin of control system on time delay of measured angular acceleration.

3 Control Law Evaluation

3.1 Evaluation Points and Method

The frequency-domain linear analysis is performed to assess stability margin of the control system with $\mathbf{K}_{\mathrm{aug}}$, synchronization filter and control surface feedback path at Mach number 0.95, 30 Kft altitude and 1 g flight condition, and to evaluate the characteristics of the structural coupling in the simulated SCT environment, which is based on the real structural noise data of sensors and control surface by gathering the ground test. In addition, the time response characteristics of the aircraft are evaluated for impulse and step control inputs in time-domain simulation environment.

3.2 Control Surface Synchronization Filter Design

In general, the angular acceleration of the aircraft can be easily obtained by differentiating the measured angular rate, but it should be noted that this differential method can amplify the noise of the measured angular acceleration. And SCF, actuator and sensor dynamics might cause an additional time delay in angular acceleration feedback. Therefore, the designer should use the low-pass filter considering sampling rate of FLCC. And, as already known, the time delay of the measured angular acceleration feedback significantly affects the performance degradation of the aircraft and the stability margin reduction of the control system [58]. These characteristics can seriously impair flight safety of the aircraft with relaxed static stability (RSS) configuration [21].

In this study, it is assumed that the angular acceleration is obtained by differentiating the angular rate measured by IMU sensor, which is usually used to production aircraft. Here, time constant of the 1st order differential filter is selected as 0.047 (3/64) considering the characteristics of noise amplification and 64 Hz sampling time of FLCC. The second-order SCF is designed on feedback path of angular acceleration to eliminate the high-frequency structural coupling effect. As mentioned earlier, the asynchronization between the measured angular acceleration and the control surface feedbacks reduces stability margin of the control system and causes aggravating instability of the aircraft. For synchronizing control surfaces feedback to eliminate time delay of the measured angular acceleration feedback, we consider 2nd or 4th order equivalent synchronization filters with a damping ratio of 0.707 on the feedback path of control surface. At this time, the frequency of the synchronization filters was optimized in two ways as follows: the first method is to optimize the frequency of synchronization filter in the dynamics of angular acceleration feedback path considering IMU sensor model measuring angular rate, differential angular rate and SCF. Another method is to optimize the frequency of the synchronization filter so that the stability margin criteria (gain margin $\geq \pm 6$ dB, phase margin $\geq \pm 45°$) can be satisfied in the linear control system environment including control law, actuator, airframe and sensor dynamics.

Figure 3 shows the gain and phase responses of the high-order and low-order equivalent synchronization filter at the control surface command feedback path, and the ones of the optimization results of synchronization filter. Here, (a) is to feedback control surface command from actuator dynamics, and (b) is to feedback control surface command from control law within the FLCC. Figure 3a depicts the result of optimizing the frequency of 2nd order synchronization filter. The black and blue solid lines show the frequency response of the high-order system considering the dynamics of the angular acceleration feedback path and 2nd order equivalent synchronization filter, and the red dotted line shows the frequency response of the 2nd order equivalent synchronization filter that satisfies stability margin of linear control system. At this time, total time delay of measured angular acceleration from actuator command to flight control feedback estimates about 70 ms, approximatively. The frequency of 2nd order equivalent synchronization filter matched with the phase response of the high-order system is 22.89 rad/s and mismatch cost value is 13, which is relatively well matched around 20 rad/s frequency band, but there is some difference in the phase response around 10 rad/s. And the frequency of synchronization filter optimized to satisfy the stability margin criteria in the linear control system is 20.3 rad/s, and the matched phase response around 10 rad/s is relatively better than 20 rad/s. Figure 3b shows the result of optimizing the frequency of 4th order equivalent synchronization filter. In this case, additional time delay occurs about 17 ms due to actuator dynamics to obtain the measured angular acceleration. The green dotted line shows the phase response of 2nd order equivalent synchronization filter matching the one of high-order system including actuator dynamics. The frequency of synchronization filter is 14.7 rad/s, but mismatch cost value is very high as 160. To improve the phase response fitting to reduce mismatch cost value, we considered 4th order synchronization filter instead of 2nd order one. The solid blue line and the dotted red line show the phase response of 4th order synchronization filter. The frequency of 4th order synchronization filter matching the phase response of the high-order system is 27.3 rad/s and mismatch cost value is 34, which is relatively well matched around 18 rad/s frequency band, but there is a difference in the phase response around 10 rad/s and above 20 rad/s. To improve the phase frequency around 10 rad/s, the frequency of synchronization filter is optimized with constraint of stability margin criteria in the linear control system. As a result, the frequency of 4th order synchronization filter is 22.9 rad/s and the matching characteristics of phase response around 10 rad/s is relatively better than above 12 rad/s. Considering these analysis result, it means that the designer should consider the gain crossover frequency of the control system when designing the frequency parameter of synchronization filter. That is, the frequency of synchronization filter should be optimized with constraints of flying qualities and stability margin criteria based on the control system. In the next section, we present the results of evaluating the stability margin evaluation on the synchronization filters and the control surface feedback path method.

3.3 Stability Margin Evaluation

The stability margins are required for the control system to allow various uncertainties in system dynamics such as mathematical modeling error in defining nominal system and plant, variations in dynamic characteristics caused by changes in environmental conditions, manufacturing tolerances, aging, wear, noncritical material failures, aircraft modifications in the post-development phase, and

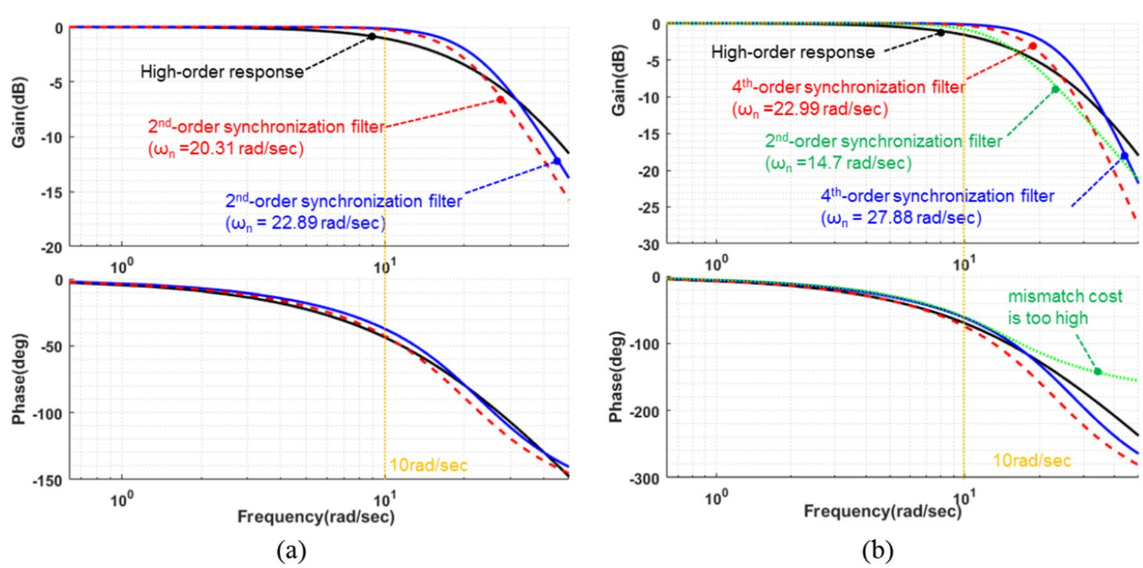

Fig. 3 Bode plot on control surface feedback path and synchronization filter optimization (high-order vs. 2nd or 4th equivalent) **a** 2nd—LOES fitting (control surface feedback in actuator dynamics), **b** 4th—LOES fitting (control surface feedback from control law within FLCC)

maintenance induced errors in calibration, installation, and adjustment [61]. To ensure the robustness of control system against various uncertainties, there have been the proposed various standards that present the requirements of stability margin; for example, the MIL-HDBK-516C [60], MIL-DTL-9490E [61], etc. In those standards, it is recommended to meet more than gain margin ± 6 dB and phase margin ± 45°. Generally, the stability margin criteria set the hard constraint that must be satisfied when optimizing control gain [59]. This section presents the evaluation results of the stability margin of the control system on synchronization filter, control surface feedback path and variation of $\mathbf{K}_{aug}$. The evaluation cases can be divided into two categories: the model-based (cases 1, 2) INDI and the hybrid INDI (cases 3–8). Here, K_{aug} of 0.0 means that the measured angular acceleration sensor signal is not used (i.e., model-based INDI), and K_{aug} of 0.6 means that the measured angular acceleration is used at 60% (i.e., hybrid INDI).

Figure 4 shows the Nichol plots for cases 1, 3, 5 and 8 in the broken loop of the pitch rate, normal acceleration, pitch angular acceleration feedback path and the horizontal control surface command path in Mach number 0.95, altitude 30 Kft, and 1 g flight condition. Among the variables fed back to the hybrid INDI control law, pitch rate and pitch angular acceleration has a significant influence on the stability margin of the control system. However, the stability margin can be increased beyond the requirement range by designing a synchronization filter in the control surface feedback path.

Table 1 and Fig. 5 show the results of stability margin evaluation in the broken loop of horizontal tail control surface on synchronization filter, control surface feedback path and variation of $\mathbf{K}_{aug}$ at Mach number 0.95, altitude 30 Kft and 1 g flight condition. The model-based INDI control (white square and diamond symbol) is not affected by synchronization filter and has a relatively enough stability margin, gain margin of 12.8 dB and a phase margin of 66.6°. And gain crossover frequency is in the relatively low frequency band at 6.1 rad/s. The hybrid INDI control significantly reduces the stability margin of the control system compared to the model-based INDI control. In case of the hybrid INDI without synchronization filter in control surface feedback path (case 3, white circle symbol), gain and phase margins are 3.0 dB and 19.5°, respectively, and the gain margin is reduced by 9.8 dB and the phase margin is reduced by 47.1° compared to the model-based INDI. If the control surface command is fed back from control law within the FLCC and the actuator dynamics is not reflected when designing 2nd order synchronization filter (case 6, black diamond symbol), the gain and phase margin are 6.1 dB and 28.2°, respectively, which does not satisfy the stability margin criteria. The case 4 (white circle symbol) and 7 (black triangle symbol) are the results of stability margin evaluation in case of control surface feedback after and before actuator dynamics, and 2nd and 4th order synchronization filters based on the frequency response of the angular acceleration feedback path, respectively. The gain margin satisfies the criteria with more than 8 dB, but the phase margin is 44.2° and 41.7°, respectively, which do not satisfy the requirement of 45° or more. The frequency response of 2nd or 4th order synchronization filters matches well around 20 rad/s compared to high-order frequency response, but there is a difference around 10 rad/s frequency band, which is gain crossover frequency, 10.9 rad/s, so the phase margins are slightly decreased. To further increase the phase margin, the frequency of synchronization filter is optimized (case 5, black square symbol and case 8, black circle symbol) to satisfy the stability margin in the control system including control law, actuator, airframe and sensor dynamics, etc. The phase margin can be further increased to more than 46° with using this optimization method of frequency of synchronization filter in the control system environment.

As an evaluation result, the stability margin can be increased up to the criteria by designing a synchronization filter in the control surface feedback command path considering the time delay of angular acceleration feedback in the hybrid INDI control method.

3.4 Structural Coupling Evaluation

The highly maneuverable military fighter aircrafts employ the RSS configuration design concept to achieve performance enhancements. A digital fly-by-wire (DFBW) flight control system (FLCS) using various sensor feedbacks such as rate, acceleration and angular acceleration measuring by IMU sensors is adopted to stabilize an unstable aircraft and attain the adequate handling qualities. Since the IMU is mounted on flexible airframe, it also measures the structural vibration with rigid body motion of the aircraft and feeds it back to the FLCC, and the structural vibration is injected as control surface actuator inputs, which then drive the controls in the frequencies of the aeroelastic modes of the aircraft [62]. Consequently, SCF [63] such as notch filters design to control law feedback path to allow the selective attenuation of the airframe structural vibration content. With modern fighter type aircraft designed to be statically unstable it is important that such SCFs do not preventing degradation to the flying qualities due to phase loss and associated time delay due to structural vibration. The structural coupling margin should be verified by SCT before flight test.

The open-loop linear control system environment including control law, airframe dynamics, actuator and sensor model is designed to emulate the SCT. The structural vibration signals including pitch rate, normal acceleration and horizon tail command are obtained from ground test and

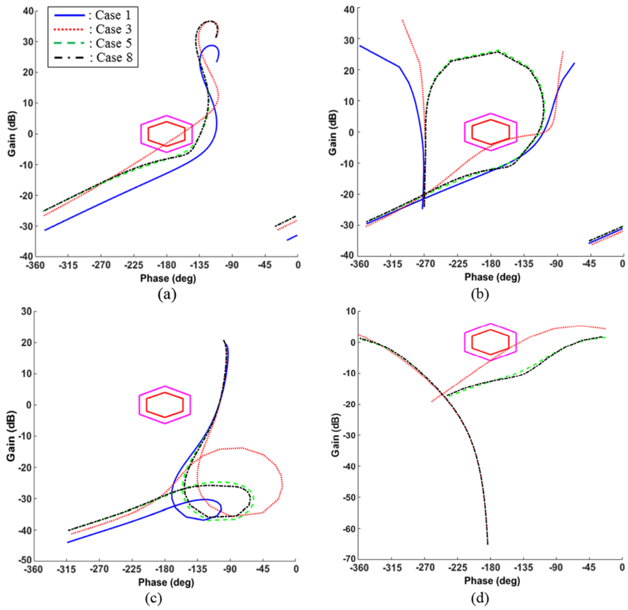

Fig. 4 Nichol plot on synchronization filter type and control surface feedback path in Mach 0.95, 30 K, 1 g level flight **a** broken loop at control surface, **b** broken loop at pitch rate, **c** broken loop at normal acceleration, **d** broken loop at pitch angular acceleration

inserted to the control surfaces command and IMU sensor feedback path. Figure 6 shows the gain margin and coherence plot according to the variation of $\mathbf{K}_{aug}$ at Mach 0.95 and altitude 30 Kft and 1 g level flight condition. Here, Fig. 6a is to feedback control surface command from actuator dynamics (cases 1, 3 and 5), and Fig. 6b is to feedback control surface command from control law within the FLCC (case 8).

Figure 6a shows the SCT evaluation result according to whether or not a synchronization filter is applied to the control surface command feedback path in the model-based and the hybrid INDI control that feedbacks control surface command from actuator dynamics. The blue solid line (case #1) indicates the structural coupling influence in the model-based INDI control, which shows the structural vibration mode around 2 Hz of the gear mode and around 10 Hz of the first structural vibration frequency, and the coherence is 0.6 or higher, ensuring the reliability of the evaluation result. Overall, the control system has an enough gain margin over − 20 dB in the model-based INDI control. The red (case #3) and green (case #5) dotted lines show the structural coupling impact on the hybrid INDI control with or without application of the synchronization filter in the control surface command feedback path. The red dotted line (case #3) is the SCT evaluation result of the hybrid INDI control without a synchronization filter. The gain margin is considerably reduced over the entire frequency range, and the coherence is quite large as 1.0 in the frequency ranges up to 30 Hz due to the influence of the control surface vibration element. For this reason, the gain margin criterion of − 6 dB is not satisfied in the frequency range below 2.5 Hz. On the other hand, the gain margin increases in the entire frequency domain when a synchronization filter is applied to the control surface feedback path (case #5). However, the coherence is still high and the gain margin is relatively reduced below 7 Hz compared to the model-based INDI control. This is a result

Table 1 Result of stability margin evaluation in the broken loop of HT control surface at Mach 0.95, 30 K and 1 g level flight condition

Cases	K_{aug}	Control surface sync. filter			Gain margin (dB)	Phase margin (°)	ω_{180} (rad/s)	Crossover Freq. (rad/s)	Remark
		Type	Freq. (rad/s)	FB. position					
1	0.0	N/A	–	Actuator dynamics	12.8	66.6	27.4	6.1	Model-based
2	0.0	2nd	22.89		12.8	66.6	27.4	6.1	
3	0.6	N/A	–		3.0	19.5	20.8	16.2	Hybrid
4	0.6	2nd	22.89		8.4	44.2	27.5	10.9	
5	0.6	2nd	20.31		8.2	46.5	27.8	10.4	
6	0.6	2nd	20.31	In FLCC	6.1	28.2	22.6	13.7	
7	0.6	4th	27.28		8.9	41.7	28.7	10.9	
8	0.6	4th	22.88		8.1	46.2	29.0	10.1	

Case 1: Do not use synchronization filter for the control surface command feedback from actuator dynamics in case of $K=0.0$ (only incremental). Case 2: Use 2nd synchronization filter for the control surface feedback command feedback from actuator dynamics in case of $K=0.0$. Case 3: Do not use synchronization filter for the control surface feedback command feedback from actuator dynamics in case of $K=0.6$ (only incremental). Case 4: Use 2nd synchronization filter for the control surface feedback command feedback from actuator dynamics in case of $K=0.6$. Case 5: Use 2nd synchronization filter for the control surface feedback command feedback from actuator dynamics in case of $K=0.6$ (re-optimization ω_n). Case 6: Use 2nd synchronization filter for the control surface feedback command feedback from control law within the FLCC in case of $K=0.6$. Case 7: Use 4th synchronization filter for the control surface feedback command feedback from control law within the FLCC in case of $K=0.6$. Case 8: Use 4th synchronization filter for the control surface feedback command feedback from control law within the FLCC in case of $K=0.6$ (re-optimization ω_n)

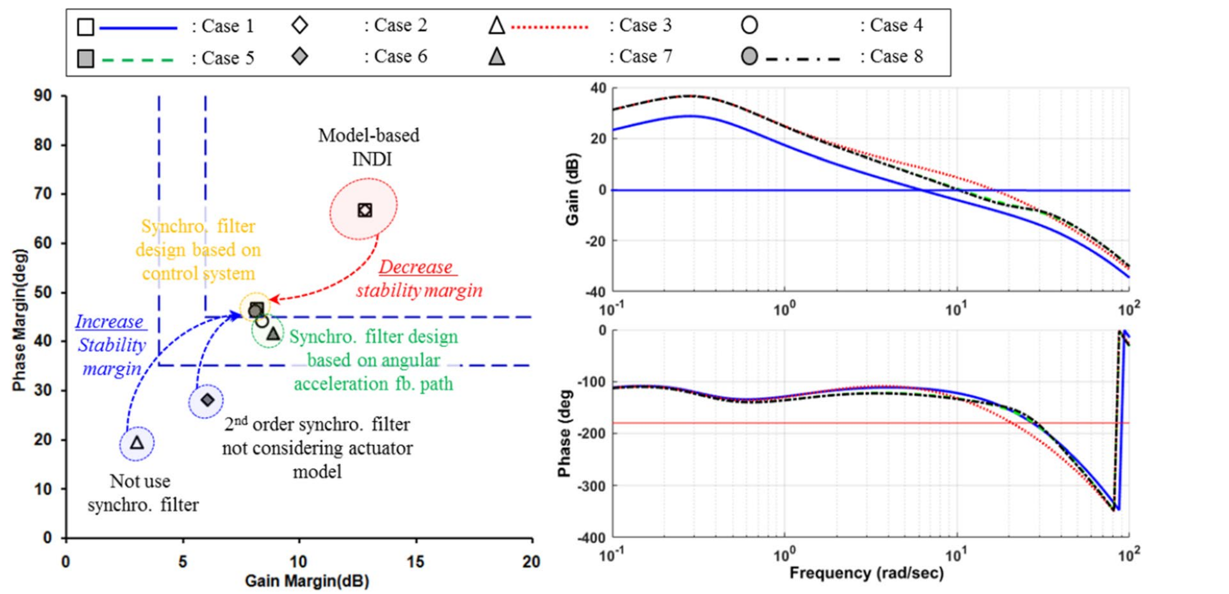

Fig. 5 Gain and phase margin (broken loop at HT control surface) on synchronization type and feedback position of control surface in Mach 0.95, 30 K, 1 g level flight

of amplitude response of the measured structural vibration when the actuator command is fed back to the flight control law.

To prevent structural vibration effect of the control surface from feeding back to the flight control law, the control surface command calculated by the control law in the FLCC is fed back instead of the control surface command in the actuator dynamics. The dashed black line (case #8) in Fig. 6b shows the SCT evaluation result in the way that the control surface command is fed back within the FLCC. As a result, the gain margin increases considerably and the coherence decreases to below 0.4 in the frequency band below 7 Hz. However, gain margin and coherence above 10 Hz frequency band have little influence on the control surface command feedback method. The structural coupling margin corresponding to the model-based INDI control can be secured by adopting this control surface command feedback method in the hybrid INDI control.

The summary of the SCT evaluation result is as follows. In case of designing the incremental INDI control, the control surface command calculated in the control law needs to be fed back within the FLCC to prevent structural vibration of the control surface from entering the control law. And the control surface feedback is synchronized in consideration of the characteristics of the actuator dynamics, IMU sensor dynamics, and differentiation of angular rate with the time delay of the angular acceleration feedback.

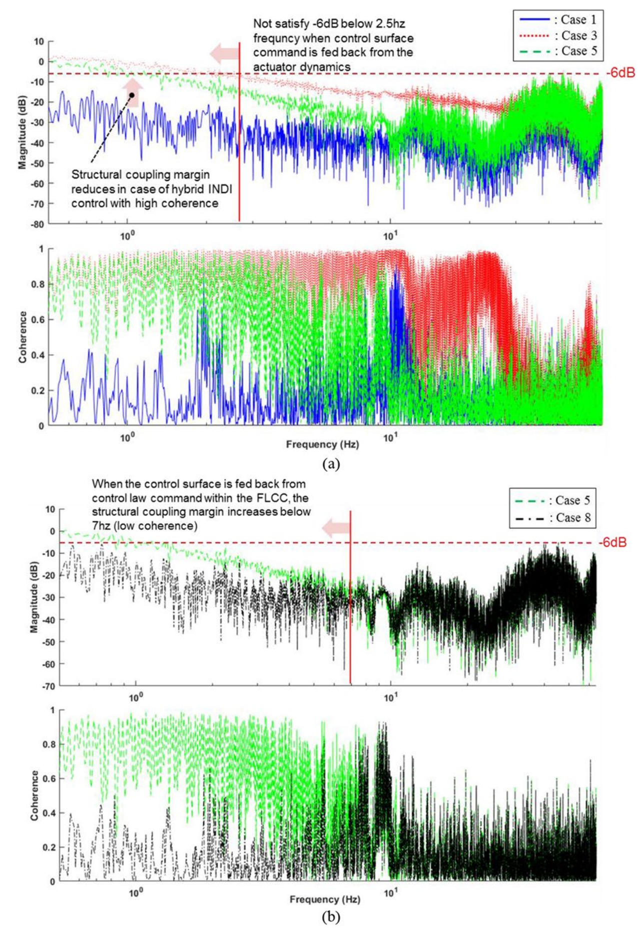

Fig. 6 Simulated structural coupling impact at Mach 0.95, 30 K, 1 g level flight **a** considering control surface command feedback from actuator dynamics, **b** considering control surface feedback from control law within the FLCC

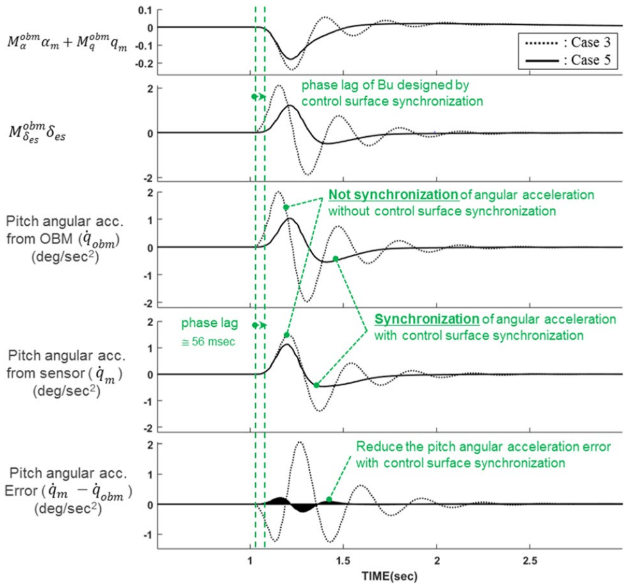

Fig. 7 Pitch angular acceleration characteristics in cases #3 and #5

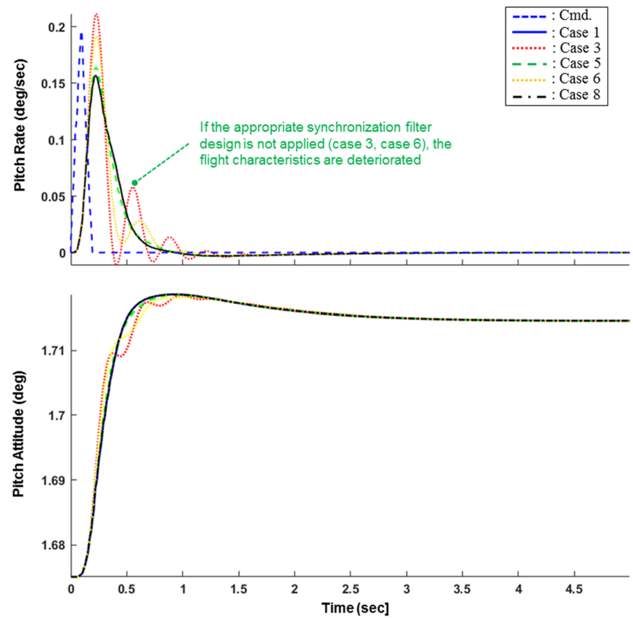

Fig. 8 Pitch rate and pitch attitude response to spike inputs

3.5 Flying Qualities Evaluation

This section presents the results of analyzing the characteristics of both the angular acceleration measured from the IMU and the angular acceleration calculated from the OBM model whether or not a synchronization filter is designed. And the result of evaluating the response of the aircraft to the impulse and step control input according to the control methods is presented.

Figure 7 shows the angular acceleration characteristics according to whether or not a synchronization filter is designed at the control surface command feedback path in the hybrid INDI control without considering initial trim values. The black dotted line shows the angular acceleration characteristics of the hybrid INDI control without applying a synchronization filter to the control surface feedback path. In this case, the angular acceleration measured from the IMU sensor has a time delay. However, there is no time delay for the $M_{\delta_{es}}^{obm}\delta_{es}$ calculated, where the control surface feedback, u and the control effectiveness matrix, $M_{\delta_{es}}^{obm}$ provided from OBM. Therefore, the calculated angular acceleration, $M_\alpha^{obm}\alpha_m + M_q^{obm}q_m$, and the measured angular acceleration from the IMU have a time gap of approximately 70 ms, which makes an error of angular acceleration up to 2.1°/s^2 and oscillation characteristics. To reduce the time gap, a synchronization filter is designed in the control surface feedback path to eliminate the time delay of about 73 ms in $M_{\delta_{es}}^{obm}\delta_{es}$. The time delay is also mentioned as time delay of measured angular acceleration in chapter "control surface synchronization filter design". As a result, the angular acceleration error is significantly reduced to 0.26°/s^2.

Figure 8 shows the response characteristics of the pitch rate and the pitch attitude to the impulse control input with a magnitude of 0.2 g for 0.2 s. The response characteristics of the model-based INDI control (case 1) and the hybrid INDI control (cases 5 and 8) that apply the synchronization filter are stabilized immediately within one overshoot after 1 s. At this time, the maximum pitch rate is 0.16°/s. On the other hand, in the hybrid INDI control that does not apply the synchronization filter (case 3) or apply the synchronization filter without considering the characteristics of the actuator dynamics (case 6), the pitch rate response increases to 0.2°/s and, the pitch rate overshoot occurs three to five times until the aircraft is stabilized. But the pitch rate and pitch attitude characteristics are similar after 1.5 s after the transient response.

Figure 9 shows the response characteristics of the aircraft to 2 g step input. In the hybrid INDI control, the normal acceleration response to the control command is similarly maintained in steady states regardless of whether synchronization filters. However, in the model-based INDI control there is a characteristic that the normal acceleration of the aircraft increases in steady state, and there is an offset of about 0.05 g after the control command release. For this reason, the aircraft cannot maintain a 20° pitch attitude, and the pitch attitude increases to 21°. This response characteristic degrades handling qualities by causing nose-up in pitch attitude capture maneuver. The pitch rate oscillation occurs

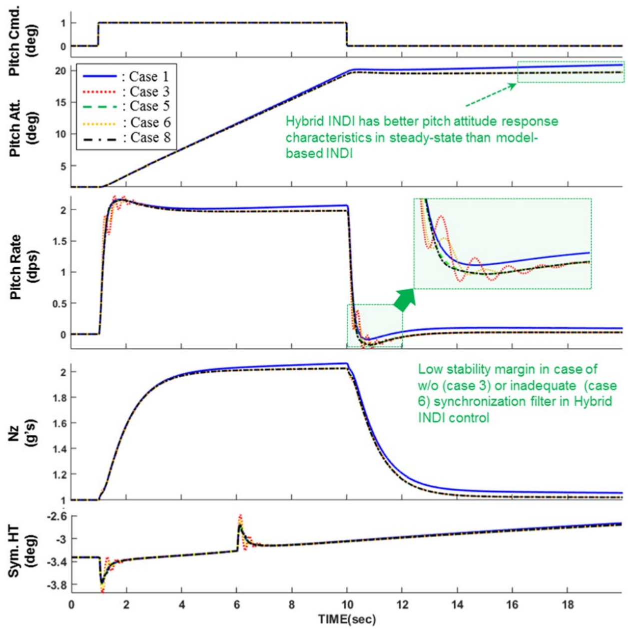

Fig. 9 Pitch axis response to step input

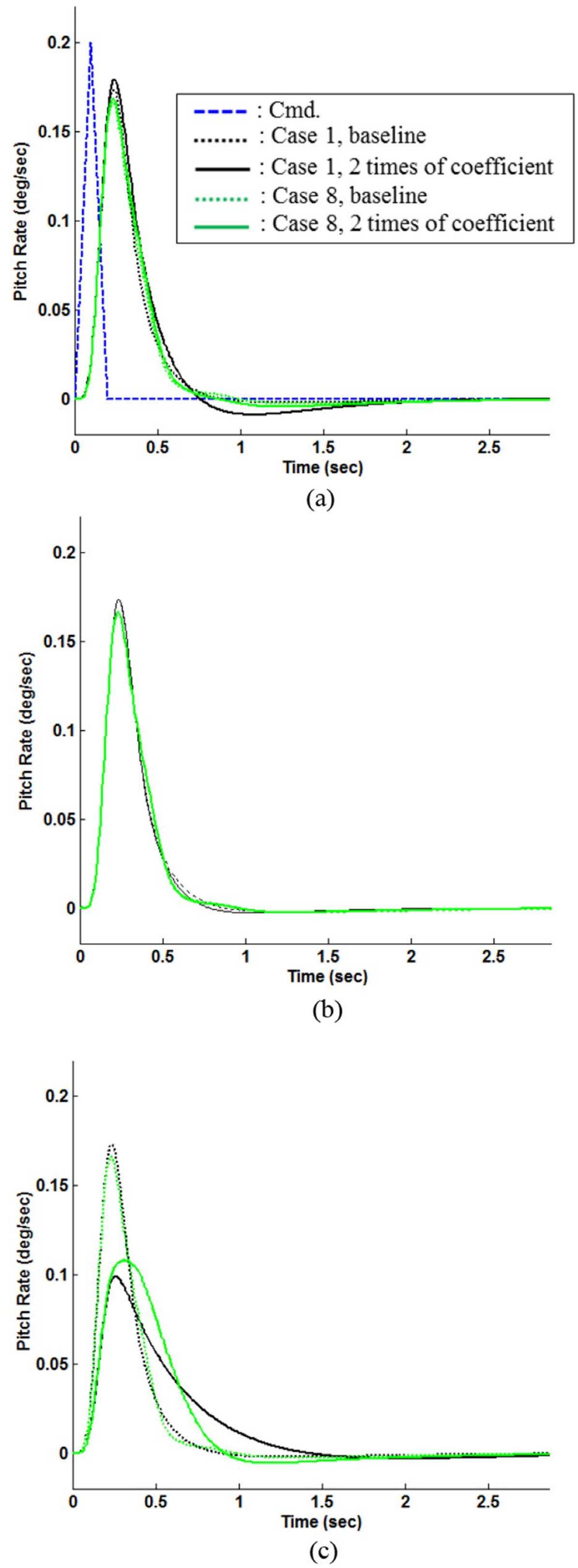

Fig. 10 Pitch rate response to aerodynamics and control effectiveness coefficient uncertainties **a** M_q, **b** M_α, **c** $M_{\delta_{es}}$

when the aircraft changes to a new pitch attitude with control input and it stabilizes within about 2 s in a steady state and this characteristic occurs due to the lack of stability margin.

This section presents the results of analyzing the sensitivity characteristics of the model-based INDI control (case 1) and the hybrid INDI control (case 8) for the uncertainties of major aerodynamics and control effectiveness coefficients. As major uncertainties coefficients, M_α, M_q, and $M_{\delta_{es}}$ representing the dynamic characteristics of the longitudinal axis were selected, and the uncertainties for each coefficient were 0.5 and 2.0. Here, 1.0 means there are no uncertainties in the coefficient. Figure 10 shows the result of evaluating the pitch rate response to the spike control input at the uncertainties of the coefficient 2.0. Here, Fig. 10a is the pitch rate response to the uncertainties of Ma, Fig. 10b is the pitch rate response to the uncertainties of M_q, and Fig. 10c is the pitch rate response to the uncertainties of $M_{\delta_{es}}$. The model-based INDI control is significantly affected by the uncertainties of M_q. However, any control method is hardly affected by the uncertainties of M_α. Overall, the hybrid INDI control is robust against uncertainties in aerodynamic coefficients compared to the model-based INDI control. This is because the angular acceleration measured from the IMU has little uncertainties in the aerodynamic coefficients. In the case of the model-based INDI control, the natural frequency of the pitch rate response is lower and the short-period damping is lower for the uncertainties of the $M_{\delta_{es}}$ coefficient. But, the two control methods are sensitive to the uncertainties of the control effectiveness coefficient, $M_{\delta_{es}}$, as shown in Fig. 9c, In general, it is possible to obtain relatively accurate control effectiveness coefficients through wind tunnel tests during aircraft development phase. However, the design method that extracts the control effectiveness coefficient in real time during flight should be considered to further improve the robustness of the aircraft against uncertainties with the hybrid INDI control method.

4 Conclusion

Modern highly maneuverable fighter aircraft satisfies the required flying qualities and stability by designing control laws with various control techniques using a mathematical model based on aerodynamic data. Most of the production fighter aircrafts use classical control techniques, but the F-35 JSF adopted the model-based INDI for the design of control law for the first time. The model-based INDI control method requires an accurate aircraft model to achieve the required flying qualities. However, it is difficult to obtain accurate aerodynamic data especially in a transonic flight condition with unsteady flow characteristics. The sensor-based INDI using angular acceleration measured from the IMU sensor is known to be a fairly robust control method for model uncertainties, which is required to overcome these complex aerodynamic characteristics. However, the time delay of the measured angular acceleration reduces the stability margin of the control system so the sensor-based IDNI is vulnerable to the structural coupling characteristics in low frequency band.

In this paper, we proposed the hybrid INDI control with additional augmentation control using the error between the angular acceleration calculated from the OBM and the angular acceleration measured from the IMU sensor, based on the model-based INDI control which was already verified in the F-35 JSF. And the control surface feedback synchronization design method was also proposed to improve the stability margin of control system. This design method is relatively simple because it can be modeled as just a second or fourth-order filter. Above all, these design methods are an efficient control method that can improve the flying qualities in the transonic flight condition by applying it to an aircraft developed with the aim of production in which it is essential to obtain airworthiness certification.

5 Future Work

The synchronization and feedback path of control surface feedback proposed in this paper is an effective method of increasing the stability margin and minimizing structural coupling characteristics of the control system. However, the proposed control method has a still have the disadvantage of decreasing the stability margin of the control system compared to the model-based INDI control. In the future, we plan to research a control algorithm that further increases the stability margin and minimizes structural coupling characteristics of control system based on the hybrid INDI control.

Acknowledgements The authors would like to deliver their sincere thanks to the editors and anonymous reviewers.

Funding This research received no specific grant from any funding agency in the public, commercial, or not-for-profit sectors.

Data Availability The data used to support the findings of this study are available from the corresponding author upon request.

Declarations

Conflict of Interest The authors declare that there is no conflict of interest regarding the publication of this paper.

References

1. Balas GJ (2003) Flight control law design: an industry perspective. Eur J Control 9(2–3):207–226
2. Balas GJ, Hodgkinson J (2009) Control design methods for good flying qualities. In: AIAA atmospheric flight mechanics conference, AIAA, Chicago, IL, USA
3. Kim C et al (2018) Development of model-/sensor-based nonlinear dynamic inversion control technique for highly maneuverability fighter. Int J Control Autom Syst 24(7):639–6540
4. Enns D, Bugajski D, Hendrick R, Stein G (1994) Dynamic inversion: an evolving methodology for flight control design. Int J Control 59(1):71–91
5. MIL-HDBK-1797:1997. Department of defense handbook flying qualities of piloted aircraft
6. Sieberling S, Chu QP, Mulder JA (2010) Robust flight control using incremental nonlinear dynamic inversion and angular acceleration prediction. J Guid Control Dyn 33(6):1732–1742
7. Simplıcio P, Pavel MD, van Kampen E, Chu QP (2013) An acceleration measurements-based approach for helicopter nonlinear flight control using incremental nonlinear dynamic inversion. Control Eng Pract 21(8):1065–1077
8. Smeur EJJ, Chu QP, de Croon GCHE (2016) Adaptive incremental nonlinear dynamic inversion for attitude control of micro air vehicles. J Guid Control Dyn 39(3):450–461
9. Miller CJ (2011) Nonlinear dynamic inversion baseline control law: flight-test results for the full-scale advanced systems Testbed F/A–18 airplane. In: American Institute of Aeronautics and Astronautics, guidance, navigation, and control conference, 8–11 Aug 2011, New York
10. Wacker R, Munday S, Merkle S (2001) X-38 application of dynamic inversion flight control. In: Proceedings of the 24th annual AAS guidance and control conference, Breckenridge, CO, 31 Jan–4 Feb 2001, Houston
11. Munday S (2000) X-38 MACH FCS overview. In: SAE Aerospace G&C, 16 Mar 2000
12. Brinker JS, Wise KA (2001) Flight testing of reconfigurable control law on the X-36 tailless aircraft. J Guid Contr Dyn 24:903–909
13. Gregory W, David A (2002) X-35B STOVL flight control law design and flying qualities. In: 2002 biennial international powered lift conference and exhibit, Williamsburg, VA, 5–7 Nov 2002, New York

14. Harris JJ, Standfords JR (2018) F-35 flight control law design, development, and verification. In: American Institute of Aeronautics and Astronautics aviation forum, 2018 aviation technology, integration, and operations conference, Atlanta, GA, 25–29 June 2018, New York
15. Smith P, Berry A (2000) Flight test experience of a nonlinear dynamic inversion control law on the VAAC harrier. In: Atmospheric flight mechanics conference, Denver, CO, 14–17 Aug 2000
16. Smith PR (19998) A simplified approach to non-linear dynamic inversion based flight control. In: Proceedings of the 1998 American Institute of Aeronautics and Astronautics, atmospheric flight mechanics conference, Boston, MA, 10–12 Aug 1998, pp 762–770
17. Buffington JM (1999) Modular control law design for the innovative control effectors (ICE) tailless fighter aircraft configuration. In: Wright-Patterson Air Force Base, OH, June 1999
18. Grondman F, Looye GHN, Kuchar R et al (2018) Design and flight testing of incremental nonlinear dynamic inversion based control laws for a passenger aircraft. In: AIAA Sci-Tech forum, Kissimmee, FL, 8–12 Jan 2018
19. van't Veld R, Van Kampen E-J, Ping Chu Q (2018) Analysis and robustness analysis and improvements for incremental nonlinear dynamic inversion control. In: AIAA, 7 Jan 2018
20. American Institute of Aeronautics and Astronautics (2018) Stability analysis for incremental nonlinear dynamic inversion control. In: American Institute of Aeronautics and Astronautics (AIAA), p 1
21. Kim C, Yang I, Sung J, Cho I, Hwang B (2018) Development of nonlinear dynamic inversion control to improve flying qualities corresponding to longitudinal CG travel in flight operation. J Inst Control Robot Syst 24(3):223–240
22. Kim C, Yang I, Koh G (2018) A study on longitudinal control law design and flying quality parameter optimization for highly maneuverable fighter. J Inst Control Robot Syst 24(8):767–776
23. Kim C, Yang I, Koh G, Kim BS (2019) Development of a robust control technique on failures of the XCG measurement sensor. J Inst Control Robot Syst 25(3):268–275
24. Kim C, Ji C, Kim BS (2020) Development of flight control law for improvement of uncommanded lateral motion of the fighter aircraft. Int J Aeronaut Space Sci 21:1059–1077
25. Kim C, Jin, T, Koh G, Kim BS (2021) Control law design to improve the unexpected pitch motion in slow down turn (SDT) maneuver. In: Proceedings of the Institution of Mechanical Engineers, Part G: Journal of Aerospace Engineering, 15 Apr 2021
26. Chambers JR, Hall RM (2003) Historical review of uncommanded lateral-directional motions at transonic conditions. In: 41st Aerospace sciences meeting & exhibit, 6–9 Jan 2003
27. Hanel M, Neuhuber W, Osterhuber R, Hofinger G, Barrio M (2004) Asymmetric stiffness pitch control - transonic pitch-up mitigation for the EF2000. In: AIAA guidance, navigation, and control conference, Providence, Rhode Island, AIAA-2004-4752, 2004
28. Pearcey HH, Holder DW (1954) Examples of the effects of shock-induced boundary layer separation in transonic flight. In: A.R.C. 16,446, 1954
29. Hall RM, Woodson SH (2004) Introduction to the abrupt wing stall (AWS) program. In: American Institute of Aeronautics and Astronautics Journal of Aircraft, vol 41, no 3, May–June 2004
30. Bruce Owens D, McConnell JK, Brandon JM, Hall RM (2004) Transonic free-to-roll analysis of the F/A-18E and F-35. In: American Institute of Aeronautics and Astronautics Atmospheric Flight Mechanics Conference and Exhibit, 16–19 Aug 2004
31. Anderson SB, Ernst EA, Van Dyke RD (1951) Flight measurements of the wing-dropping tendency of a straight-wing jet airplane at high subsonic Mach numbers. In: NACA RM A51 628, 1951
32. McFadden NM, Rathert GA, Bray RS (1955) The effectiveness of wing vortex generators in improving the maneuvering characteristics of a swept-wing airplane at transonic speeds. In: NACA TN 3523, 1955
33. (1975) The effects of buffeting and other transonic phenomena on maneuvering combat aircraft. In: Advisory Group for Aerospace Research and Development, July 1975
34. Rahn R (1983) Oversimplification can sometimes be hazardous to your health-the XA4D Skyhawk Story. In: Society of experimental test pilots symposium
35. Phillips EH (1989) Team correcting deficiencies in Navy's T-45A trainer aircraft. In: Aviation week and space technology, 30 Oct 1989
36. Friend EL, Sefic WJ (1972) Flight measurements of buffet characteristics of the F-104 airplane for selected wing-flap deflections. In: NASA TN D-6943, National Aeronautics and Space Administration, Washington, DC, Aug 1972
37. Monaghan RC, Friend EL (1973) Effects of flaps on buffet characteristics and wing-rock onset of an F-8C airplane at subsonic and transonic speeds. In: NASA TM X-2873, 1973
38. Hanley RJ (1987) Development of an airframe modification to improve the mission effectiveness of the EA-68 airplane. In: American Institute of Aeronautics and Astronautics, 87-2358, 1987
39. Chambers JR, Anglin EL (1969) Analysis of lateral-directional stability characteristics of a twin-jet fighter airplane at high angles of attack. In: NASA TN D-5361, 1969
40. Ray EJ, Hollingsworth EG (1973) Subsonic characteristics of a twin-jet swept-wing fighter model with maneuvering devices. Feb 1973
41. (1979) Manoeuvre limitations of combat aircraft. In: AGARD Advisory Report, No. 155A
42. Hwang C, Pi WS (1974) Investigation of Northrop F-5A wing buffet intensity in transonic flight. In: NASA Contractor Report 2484, Nov 1974
43. Hwang C, Pi WS (1978) Investigation of steady and fluctuating pressures associated with the transonic buffeting and wing rock of a one-seventh scale model of the F-5A aircraft. In: NASA Contractor Report 3061, Nov 1978
44. Hwang C, Pi WS (2012) Some observations on the mechanism of aircraft wing rock. In: American Institute of Aeronautics and Astronautics Aircraft Systems and Technology Conference, Los Angeles, CA, 22 May 2012
45. Lusby WA, Hanks NJ (1961) T-38A category II stability and control tests. In: AFFTC-TR-61-15, Aug 1961
46. Friend EL, Sakamoto GM (1978) Flight comparison of the transonic agility of the F-111A airplane and the F-111 supercritical wing airplane. In: NASA TP 1368, 1978
47. Bore CL (1972) Post-stall aerodynamics of the harrier GRl. In: AGARD-CP-102 fluid dynamics of aircraft stalling
48. Moss GF (1979) Some UK research studies of the use of wing-body strakes on combat aircraft configurations at high angles of attack
49. Stevenson SL, Holl D, Roman A (1992) Parameter identification of AV-86 Wingborne aerodynamics for flight simulator model updates. In: American Institute of Aeronautics and Astronautics, 92-4506-CP, 1992
50. O'Leary CO (1977) Wind-tunnel measurement of lateral aerodynamic derivatives using a new oscillatory rig with results for the Gnat aircraft. In: RAE Technical Report 771 59
51. Sisk TR, Matheny NW (1979) Precision controllability of the F-15 airplane. In: NASA Technical Memorandum TM-72861, May 1979
52. Davison MT (1992) An examination of wing rock for the F-15. Master's Thesis, Air Force Institute of Technology, AFIT/GAE/ENY/92M-O11, Feb 1992

53. Sisk TR, Matheny NW (1980) Precision controllability of the YF-17 airplane. NASA Technical Paper TP-1677, May 1980
54. Traven R, Hagan J, Niewoehner R (1998) Solving wingdrop on the F-18E/F super hornet. In: Proceedings of the 42nd symposium aerospace and high technology database, society of experimental test pilots, Lancaster, CA, Sept 1998, pp 67–84
55. Luo J, Lan EC (1993) Control of the wing rock motion of slender delta wings. J Guid Control Dyn 16(2):225–231
56. Shue SP, Sawan ME, Rokhsaz K (1996) Optimal feedback control of a nonlinear system: wing rick example. J Guid Control Dyn 19(1):166–171
57. Kim C, Ji C, Kim BS (2020) Development of a control law to improve the handling qualities for short-range air-to-air combat maneuvers. Adv Mech Eng 12(7):168781402093679
58. van 't Veld RC, van Kampen E, Chu QP (2018) Stability and robustness analysis and improvements for incremental nonlinear dynamic inversion control. In: American Institute of Aeronautics and Astronautics, 7 Jan 2018
59. Berger T, Tischler MB (2013) Lateral/directional control law design and handling qualities optimization for a business jet flight control system. In: American Institute of Aeronautics and Astronautics atmospheric flight mechanics conference, Boston, MA, 19–22 Aug 2013, pp 1–40
60. Department of Defense Handbook - Airworthiness Certification Criteria, MIL-HDBK-516C, 12 Dec 2014
61. (2008) Flight control systems - design, installation and test of piloted aircraft, general specification for. In: MIL-DTL-9490E, 22 Apr 2008
62. Battipede M, Gili P (2009) Constrained notch filter optimization for a fly-by-wire flight control system. J Aerosp Sci Technol Syst 88:105–113
63. Burge SE, Felton RD (1996) Reduction of structural coupling in advanced fighter aircraft by active structural mode control. In: UKACC international conference on control '96 (Conf. Publ. No. 427), Exeter, UK, vol 1, pp 626–631. https://doi.org/10.1049/cp:19960624